

# Real-Time Learning of Predictive Dynamic Obstacle Models for Robotic Motion Planning

Stella Kombo<sup>1</sup>, Masih Haseli<sup>1</sup>, Skylar Wei<sup>2</sup>, and Joel W. Burdick<sup>1</sup>

**Abstract**—Autonomous systems often must predict the motions of nearby agents from partial and noisy data. This paper asks and answers the question: “can we learn, in real-time, a nonlinear predictive model of another agent’s motions?” Our online framework denoises and forecasts such dynamics using a modified sliding-window Hankel Dynamic Mode Decomposition (Hankel-DMD). Partial noisy measurements are embedded into a Hankel matrix, while an associated Page matrix enables singular-value hard thresholding (SVHT) to estimate the effective rank. A Cadzow projection enforces structured low-rank consistency, yielding a denoised trajectory and local noise variance estimates. From this representation, a time-varying Hankel-DMD *lifted* linear predictor is constructed for multi-step forecasts. The residual analysis provides variance-tracking signals that can support downstream estimators and risk-aware planning. We validate the approach in simulation under Gaussian and heavy-tailed noise, and experimentally on a dynamic crane testbed. Results show that the method achieves stable variance-aware denoising and short-horizon prediction suitable for integration into real-time control frameworks.

## I. INTRODUCTION

Autonomous robotic systems often operate in environments where other dynamic and non-coordinated agents operate. For example, autonomous cars must navigate around vehicles, pedestrians, and cyclists [1], [2]. In autonomous drone racing, drones must avoid crashing into other drones on the racecourse [3], [4] and in maritime robotics, a shipboard robotic arm or autonomous crane must plan for the payload’s motion while compensating for the ship’s sea-induced oscillations. In such settings, the other agent’s dynamics and intentions are typically unknown while onboard sensing provides noisy, partial observations. Safe, efficient behavior therefore hinges on accurate short-horizon prediction under uncertainty to enable collision-free planning and real-time control. Thus, this paper introduces a data-driven framework for real-time learning and short-horizon prediction from noisy, partial observations.

*Related Work:* Different approaches have been developed for integrating prediction and planning in dynamic environments where other agents’ dynamics and intentions are unknown. Classical geometric planners such as the Velocity-Obstacle (VO) family [5], Reciprocal VO (RVO), Optimal Reciprocal Collision Avoidance (ORCA) and Acceleration

\*This work was supported by the Defense Advanced Research Projects Agency (DARPA) under the LINC program.

<sup>1</sup>Stella Kombo, Masih Haseli, and Joel W. Burdick are with the Division of Engineering and Applied Science, California Institute of Technology, Pasadena, CA 91125, USA. {skombo, mhaseli, jburdick}@caltech.edu

<sup>2</sup>Skylar Wei is with Applied Intuition, Mountain View, CA 94041, USA. skylar@applied.com

Velocity Obstacles extensions (AVO)) [6]–[9], embed simple relative-motion estimates to predict collisions and select controls outside forbidden sets. These methods are efficient but assume simplified behavior models and near-perfect state estimates. However, real agents often violate these assumptions. For instance, some thrown objects may be roughly ballistic [10], but aerodynamically complex bodies, e.g., frisbees, do not follow a simple ballistic model. Additionally, behavior-driven agents, e.g., pedestrians, require data-driven intent models to capture variability beyond constant-velocity assumptions [11]. Lastly, constraint-driven agents, e.g., autonomous vehicles, have future trajectories restricted by road geometry and traffic rules. Across all these instances, VO-style methods assume perfect knowledge of other agents’ states (exact positions and velocities with instantaneous updates) and neglect measurement noise or sensing delays [12]. This reliance on idealized assumptions highlights the gap between geometric formulations and the stochastic, nonlinear realities of robotics applications.

When other agents’ dynamics are unknown, it is desirable to learn predictive models online from streaming observations. In practice, only partial and noisy measurements are available, while key latent states are unobserved, degrading forecasts and the safety of plans. Prior methods assume full-state observability for simplicity [13]. This includes frameworks that learn dynamics directly from data *offline*, e.g., classical AutoRegressive Moving Average (ARMA) models [14], modern sequence learners such as Recurrent Neural Networks (RNNs), transformers and tokenized representations [15]. These off-line methods capture complex behavior but require large datasets and retraining [16] and adapt poorly to distribution shift [17]. *Online* variants update models during deployment, e.g., Kalman filtering, recursive least squares, and online Gaussian processes [18], but typically presume known or structured noise distributions [19].

Koopman theory is a complimentary alternative to learning these dynamic models. Formally, the Koopman operator models a nonlinear dynamical system via a *linear operator* on a vector space of functions [20]. Since the operator acts on an infinite dimensional vector space, real-time analysis and prediction is intractable. A practical approach is to *approximate* the operator’s action on a finite-dimensional subspace (which is typically of greater dimension than the state-space of the nonlinear system), enabling the use of well-developed methods from linear algebra and linear system theory. These approximations are often performed via orthogonal projections on the subspace of choice, also referred to as truncations of the operator’s action. Dynamic Mode

Decomposition (DMD) [21] and its variant Extended-DMD (EDMD) [22] are well-known examples of such projection-based algorithms. Hankel-DMD uses time-delay embedding to estimate an effective state-space dimension [23], [24]. Such truncated Koopman-based models offer computationally feasible approximations of nonlinear dynamics with proven utility in robotics for prediction and control [25], [26]. However, sensor measurements may be noisy and given that the fidelity of real-time Koopman predictors depends on data quality, noise degrades these learned models.

Existing denoising frameworks to resolve noisy measurements prior to model fitting include classical low-rank denoising techniques i.e., truncated Singular Value Decomposition (tSVD), Principal Component Analysis (PCA) [27] and Proper Orthogonal Decomposition (POD) [28] provide optimal projections but rely on *ad hoc* rank selection. Structured Hankel denoising [29] enforces temporal consistency but requires tuning and degrades under non-Gaussian noise. Scalable variants like randomized SVD [30] improve efficiency but depend on problem-specific thresholds, while Eigensystem Realization Algorithm (ERA) [31] and Singular Spectrum Analysis (SSA) [32] remain sensitive to noise.

**Contribution:** We propose an adaptive, denoising, sliding-window Hankel-DMD framework for real-time prediction from noisy partial measurements. At each step, a finite buffer fits a local model, balancing responsiveness to non-stationary behavior with enough samples for reliability. We first denoise via Cadzow's structured low-rank projection, with rank  $\hat{r}$  chosen by Singular Value Hard Thresholding (SVHT) on a Page embedding. We prove that, under mild conditions, Page and Hankel have the same finite-sample rank, so the SVHT choice transfers to the Hankel matrix for Cadzow denoising. The resulting denoised Hankel matrices yield a sequence of local models and noise-variance estimates for uncertainty-aware planning. We validate the framework in both simulation and hardware experiments under Gaussian and non-Gaussian correlated heavy-tailed noise and we show that the framework offers robust denoised prediction results suitable for real-time control and planning tasks.

**Notation:**  $\mathbb{R}$  and  $\mathbb{N}$  denote real and natural numbers.

$I_n$  and  $0_{m \times n}$  to denote the  $n \times n$  identity matrix and  $m \times n$  zero matrix, respectively. For matrix  $A \in \mathbb{R}^{m \times n}$ ,  $A^\top$ ,  $A^\dagger$ , and  $\text{rank}(A)$  denote its transpose, Moore–Penrose pseudo-inverse, and rank respectively. Given vector  $v \in \mathbb{R}^n$ , we denote by  $\text{diag}(v)$ , the  $n \times n$  diagonal matrix with elements of  $v$  on its main diagonal. Given vectors  $\{v_1, \dots, v_k\} \subset \mathbb{R}^n$ , we denote the set comprised of all their linear combinations by  $\text{span}\{v_1, \dots, v_k\}$ .

For a random variable  $X$ , we denote its variance by  $\sigma_X^2$  and we drop the subscript when the context is clear. Given functions  $f$  and  $g$  with matching domain and co-domain, we denote the composition by  $f \circ g(x) := f(g(x))$ .

## II. PROBLEM DEFINITION

Consider a robot that operates in the vicinity of another moving entity  $\mathcal{O}$  whose behavior and dynamics are unknown. The robot's onboard sensors detect  $\mathcal{O}$  and provide noisy,

partial measurements of the obstacle, denoted by  $x_t \in \mathbb{R}^{n_x}$ , which are sampled at a uniform interval  $\Delta t \geq 0$ , and capture kinematic quantities such as velocities or angular rates. While  $x_t$  may not directly encode full Cartesian position, it carries sufficient temporal information to enable short-horizon motion prediction. The motion of  $\mathcal{O}$  is governed by a discrete-time dynamical system with latent (unobserved) variables and unmeasured control inputs in the form:  $z_{t+1} = \hat{f}(z_t, u_t)$  where  $z_t$  denotes the state, which may include latent (unobserved) variables and  $u_t$  an input from an unknown policy  $u_t = c(z_t)$ . This induces an autonomous system  $f$  as

$$\begin{aligned} z_{t+1} &= f(z_t), \\ x_t &= C z_t + \eta_t, \end{aligned} \quad (1)$$

where  $\eta_t \in \mathbb{R}^{n_x}$  is measurement noise (unknown distribution), and  $C$  defines the state-output map. In robotics, this discrete map typically arises from discretization (or discrete sampling) of a continuous-time system. We maintain a sliding buffer of  $N$  recent measurements  $\mathcal{B}_t = \{x_{t-N+1}, \dots, x_t\}$  for online processing.

**Problem Statement:** Given streaming noisy observations  $\{x_t\}$  from a single trajectory and a sliding data buffer of fixed length  $N$ , our objective is to construct, in real time, a tractable and adaptive local model. This model should produce multi-step forecasts of future measurements  $\{\bar{x}_{t+1}, \dots, \bar{x}_{t+N_h}\}$  over a prediction horizon  $N_h \in \mathbb{N}$ , in a manner suitable for downstream tasks such as prediction, planning, and control.

## III. PRELIMINARIES

Here, we define key concepts that are leveraged in our method such as Hankel and Page embeddings, Hankel-DMD, Cadzow denoising, and Singular Value Hard Thresholding.

### A. Hankel and Page Matrices

Guided by Takens' delay-embedding theorem, that the dynamics of a system can be reconstructed from delay-coordinate maps of a single observable when the embedding dimension is sufficiently large [33], we apply delay embedding to the output measurements to extract informative structure from the system. Given a sequence of  $N$  measurements  $\{x_{i-N+1}, \dots, x_i\} \subset \mathbb{R}^{n_x}$ , we denote the associated (block) *Hankel* matrix  $H_{i-N+1:i}^L \in \mathbb{R}^{(Ln_x) \times (N-L+1)}$  by:

$$H_{i-N+1:i}^L = \begin{bmatrix} x_{i-N+1} & x_{i-N+2} & \cdots & x_{i-L+1} \\ x_{i-N+2} & x_{i-N+3} & \cdots & x_{i-L+2} \\ \vdots & \vdots & \ddots & \vdots \\ x_{i-N+L} & x_{i-N+L+1} & \cdots & x_i \end{bmatrix} \quad (2)$$

The (block) *Page*<sup>1</sup> matrix  $P_{i-N+1:i}^L \in \mathbb{R}^{(Ln_x) \times m}$  partitions the same sequence into  $m$  non-overlapping blocks of length  $L$  (with  $m = N/L$ )<sup>2</sup>:

<sup>1</sup>For  $n_x = 1$ , the matrices  $H_{i-N+1:i}^L$  and  $P_{i-N+1:i}^L$  take Hankel and Page forms, respectively. For  $n_x > 1$ , they become block Hankel and block Page. For simplicity, we refer to both cases as Hankel and Page structures.

<sup>2</sup>Note that, unlike the Hankel matrix, in the Page matrix, the buffer length  $N$  must be a multiple of the embedding window length  $L$ .

$$P_{i-N+1:i}^L = \begin{bmatrix} x_{i-N+1} & x_{i-N+L+1} & \cdots & x_{i-L+1} \\ x_{i-N+2} & x_{i-N+L+2} & \cdots & x_{i-L+2} \\ \vdots & \vdots & \ddots & \vdots \\ x_{i-N+L} & x_{i-N+2L} & \cdots & x_i \end{bmatrix} \quad (3)$$

### B. Hankel-DMD

Here, we review a variant of Hankel-DMD (cf. [23], [24]) suitable for our problem based on the delay embedding of the observables which measure the output of the dynamical system (1).

Given the measurement sequence  $\{x_0, x_1, \dots, x_n\}$ , form the one step shifted Hankel matrices  $H_{0:n-1}^L$  and  $H_{1:n}^L$  according to notation in (2). Note that the columns of  $H_{1:n}^L$  can be generated by pushing the columns of  $H_{0:n-1}^L$  one time step forward in time. To estimate the one-step propagator, Hankel-DMD relies on the following least Frobenius-norm problem in the delay coordinates,

$$A^* = \arg \min_A \|H_{1:n}^L - AH_{0:n-1}^L\|_F. \quad (4)$$

The closed form solution for  $A^*$  is

$$A^* = H_{1:n}^L (H_{0:n-1}^L)^\dagger \quad (5)$$

Under standard assumptions of ergodicity and noise-free observables, Hankel-DMD can be used as a finite-dimensional approximation of the Koopman operator via delay embeddings [23]. Our goal is to tackle the real-world cases where these assumptions do not hold.

### C. Cadzow Algorithm for Denoising

Here, we review a variant of Cadzow's algorithm for denoising Hankel matrices [34]. In *lifted* dynamics that are approximately linear (e.g., Koopman-based approximations), noise-free data lives on a low-dimensional vector space. Hence, for sufficiently large delay embedding window  $L$ , the noise-free Hankel trajectory matrix becomes low rank. However, with measurement noise, the observed Hankel matrix is generally full rank. Formally, let  $H^L \in \mathbb{R}^{(L n_x) \times (N-L+1)}$  be a Hankel matrix constructed from  $N$  consecutive noisy measurements with embedding window  $L$ . Decompose  $H^L$  as  $H^L = \hat{H}^L + \Delta$  with

$$\text{rank}(\hat{H}^L) = r < \min\{Ln_x, N-L+1\} \quad (6)$$

where  $\Delta$  denotes measurement noise and  $\hat{H}^L$  is the noise-free Hankel matrix. The objective is to recover the (unknown) noise-free, low-rank Hankel matrix  $\hat{H}^L$  from  $H^L$ . The Cadzow algorithm tries to achieve this objective by alternating between projecting  $H^L$  on the set of matrices with rank of at most  $r$  and then projecting the result back on the set of Hankel matrices as we explain below.

Given a target rank  $r$ , define the projection map  $\Pi_r$  onto the set of rank- $\leq r$  matrices as

$$\Pi_r(H) := \arg \min_{\text{rank}(Y) \leq r} \|H - Y\|_F^2 = U \Sigma_r V^\top \quad (7)$$

where  $H = U \Sigma V^\top$  is the SVD and  $\Sigma_r$  is created by keeping the top  $r$  singular values in  $\Sigma$  while setting the rest to zero. The closed-form solution of (7) is a direct consequence of Eckart–Young–Mirsky theorem, see e.g. [35]. Similarly, we define the projection map  $\Pi_H$  onto the set of Hankel matrices as

$$\Pi_H(M) := \arg \min_{Z \in \text{Hankel}} \|M - Z\|_F^2. \quad (8)$$

Interestingly, the optimization problem (8) has a closed-form solution which can be calculated by replacing the members of each anti-diagonal of  $M$  with their average. The procedure is as follows: decompose  $M$  into  $L$  by  $N-L+1$  blocks similarly to the Hankel matrix<sup>3</sup>. And denote by  $M_{i,j}$  the  $ij$ th block. For each anti-diagonal offset  $d = 0, \dots, N-1$ , define:  $\mathcal{I}_d = \{(\ell, m) : 1 \leq \ell \leq L, 1 \leq m \leq N-L+1, \ell+m-2 = d\}$  where  $s_d = |\mathcal{I}_d|$  is number of elements in  $\mathcal{I}_d$ . Then, the anti-diagonal averaging can be computed as

$$(\Pi_H(M))_{\ell,m} = \frac{1}{s_{\ell+m-2}} \sum_{(i,j) \in \mathcal{I}_{\ell+m-2}} M_{i,j},$$

for  $1 \leq \ell \leq L$ ,  $1 \leq m \leq N-L+1$ . The Cadzow algorithm successively applies the projections  $\Pi_r$  and  $\Pi_H$  so that the sequence converges to a Hankel matrix,  $\hat{H}^L$ , that is approximately of rank  $r$ . The solution of the Cadzow algorithm on  $H^L$  after  $n$  iterations is  $[\Pi_H \circ \Pi_r]^n (H^L)$  where  $[\Pi_H \circ \Pi_r]^n$  denotes the map created by composing  $\Pi_H \circ \Pi_r$ ,  $n$ -times with itself.

Notably, since the effects of projections  $\Pi_r$  and  $\Pi_H$  can be computed in closed form, the Cadzow algorithm is an attractive choice for real-time denoising, as only a few iterations are sufficient for a reasonable signal-to-noise ratio.

### D. Singular Value Hard Thresholding (SVHT)

Here we review a variant of Gavish and Donoho's result [36]. Consider a sequence (indexed by  $a$ ) of noisy matrices  $Y_a = X_a + Z_a/\sqrt{n_a}$  where  $Y_a \in \mathbb{R}^{m_a \times n_a}$  denotes a noisy matrix,  $X_a$  the "true" low-rank matrix, and  $Z_a$  denotes the noise matrix whose entries are i.i.d. zero-mean, unit-variance entries with finite fourth moment. As  $a \rightarrow \infty$ , the aspect ratio  $m_a/n_a$  converge to  $\beta \in (0, 1]^4$ .

Given the SVD  $Y_a = U \Sigma V^\top$  and a threshold  $\tau$ , we approximate the true matrix  $X_a$  by  $\hat{X}_a = U \Sigma_{\geq \tau} V^\top$  where  $\Sigma_{\geq \tau}$  is created by setting the elements of  $\Sigma$  that are less than  $\tau$  to zero.

Gavish and Donoho showed that the Asymptotic Mean Squared Error (AMSE)-optimal threshold for the data singular values depends only on the aspect ratio through the constant  $\lambda^*(\beta)$ :

$$\lambda^*(\beta) = \sqrt{2(\beta+1) + \frac{8\beta}{(\beta+1) + \sqrt{\beta^2 + 14\beta + 1}}}. \quad (9)$$

<sup>3</sup>Note that each block is a column vector with  $n_x$  rows similarly to Eq. (2)

<sup>4</sup>Following [36],  $a$  indexes a growing problem sequence with  $Y_a \in \mathbb{R}^{m_a \times n_a}$ ,  $m_a/n_a \rightarrow \beta$ , and  $Y_a = X_a + Z_a/\sqrt{n_a}$ . Their AMSE-optimal results are asymptotic as  $a \rightarrow \infty$ .

For the noise standard deviation  $\sigma$ , the optimal threshold is:

$$\tau^* = \lambda^*(\beta) \sigma \sqrt{n_a}. \quad (10)$$

When  $\sigma$  is unknown, the optimal threshold can be estimated using a data-driven approach through the Marchenko–Pastur (MP) law [37], which gives the limiting eigenvalue distribution of  $(1/n_a) Z_a Z_a^\top$  as  $m_a/n_a \rightarrow \beta$ :

$$p_\beta(\delta) = \frac{\sqrt{(\delta_+ - \delta)(\delta - \delta_-)}}{2\pi\beta\delta} \mathbf{1}_{[\delta_-, \delta_+])(\delta)},$$

with  $p_\beta(\delta) = 0$  outside  $[\delta_-, \delta_+]$ . The median of the MP distribution denoted by  $\mu_\beta$  depends only on  $\beta$  and provides a normalization for estimating the noise level  $\sigma$ . Taking  $s_{\text{med}}$  as the median of the observed singular values, the data-driven AMSE-optimal threshold can thus be estimated as:

$$\tau^*(\beta) = \frac{\lambda^*(\beta)}{\sqrt{\mu_\beta}} s_{\text{med}}. \quad (11)$$

which remains asymptotically optimal under general white noise (i.i.d., zero mean, unit variance, finite fourth moment) with the same risk as in the Gaussian case [36, Sec. VI].

#### IV. ADAPTIVE HANKEL-DMD FOR NOISY DATA

Here, we address the problem outlined in Sec. II. To enable real-time learning and prediction, we consider the use of Hankel-DMD (cf. Sec. III-B). However, applying Hankel-DMD in robotics presents two key challenges:

- **Sensor noise:** the data collected from sensors are typically noisy, which contaminates both matrices  $H_{0:n-1}^L$  and  $H_{1:n}^L$ . This is problematic because, in least-squares schemes such as (4), noise in both data matrices leads to biased or inconsistent estimators [38];
- **Ergodicity and long trajectory data requirements:** as noted in Sec. III-B, leveraging the connections between Hankel-DMD and the Koopman operator to capture global dynamics often requires ergodicity and access to long trajectories. These assumptions, however, rarely hold in robotics applications.

In what follows, we first tackle the issue of noise by introducing a denoising scheme for Hankel matrices. We then propose an adaptive sliding-window variation of Hankel-DMD that updates the model in real time as new data arrive. This approach ensures that the model remains accurate within the operating region as the system's state evolves over time.

##### A. Denoising Hankel Matrices

Consider measurements  $\mathcal{B}_t = \{x_{t-N+1}, \dots, x_t\}$  for buffer size  $N$ , collected up to time  $t$ . From this window, we construct a Hankel matrix  $H_{t-N+1:t}^L$  according to Eq. (2). Since the measurements are noisy, our goal is to denoise the Hankel matrix  $H_{t-N+1:t}^L$  via the Cadzow algorithm as described in Sec. III-C. A key step in the Cadzow algorithm is the low-rank projection  $\Pi_r$  in Eq. (7), which requires knowledge of the effective rank  $r$  of the noise-free Hankel matrix. In practice, however, this rank is typically unknown and must be estimated. An arbitrary choice of the rank can cause either over-smoothing (if underestimated) or noise

amplification (if overestimated). To avoid this, we adopt a principled, data-driven rank selection strategy based on Singular Value Hard Thresholding (SVHT) (Sec. III-D). However, the SVHT framework assumes i.i.d. noise, an assumption that is generally violated in Hankel matrices due to repeated entries. To address this, we employ Page matrices (Eq. (3)), which partition the measurement buffer into non-overlapping blocks, thereby avoiding redundancy.

1) *Step 1: Page–Hankel Rank Transfer:* As a first step toward estimating the rank of the noise-free Hankel matrix using SVHT on Page matrices, we show that, under mild conditions, the Page and Hankel embeddings of the *same* noise-free measurement buffer share the same rank.

**Lemma 1** (Page–Hankel Rank Equivalence). *Consider a locally valid linear output model*

$$z_{k+1} = Az_k, \quad x_k = Cz_k,$$

with  $z_k \in \mathbb{R}^{n_z}$ ,  $A \in \mathbb{R}^{n_z \times n_z}$ , and  $C \in \mathbb{R}^{n_x \times n_z}$ . Let  $\{x_0, \dots, x_{N-1}\} \subset \mathbb{R}^{n_x}$  be the noise-free measurements generated by the system above from the initial condition  $z_0$ . Let  $L \geq n_z$  be the embedding window and let  $N = dL$ , with  $d \geq L$ . Define<sup>5</sup>  $B = (A)^L$  and let  $P^L$  and  $H^L$  be the block Page and Hankel matrices constructed via the data. Then,  $\text{rank}(P^L) = \text{rank}(H^L)$  if

$$\text{span}\{z_0, Bz_0, \dots, (B)^{d-1}z_0\} = \mathbb{R}^{n_z}.$$

The proof is deferred to the Appendix.

Lemma 1 provides a convenient way to connect the rank of Page and Hankel embedding of noise-free measurement buffers. Before proceeding to rank estimation, we briefly explain that the conditions of Lemma 1 are mild. First, it is worth noting that with a sufficiently high sampling frequency, the system states associated with a given measurement buffer cluster within a small region of the state space, where a local linear model can accurately approximate the system's behavior. In addition, the condition  $\text{span}\{z_0, Bz_0, \dots, (B)^{d-1}z_0\} = \mathbb{R}^{n_z}$  is generic<sup>6</sup> and holds for almost all matrices  $B$  and vectors  $z_0$ .

Now, with Lemma 1 at our disposal, we can estimate the rank of the noise-free Hankel matrix associated with  $H_{t-N+1:t}^L$  by applying SVHT on the Page matrix constructed with the same data sequence.

2) *Rank Estimation using SVHT:* To apply the SVHT (cf. Sec. III-D) on the Page matrix, the number of rows in the matrix should be less than or equal to the number of columns. Therefore, for the rest of the paper, we consider the buffer length  $N = mL_n$ , with  $m \geq L_n$ . Note that this choice already satisfies the size condition in Lemma 1.

Now, construct the Page matrix  $P_{t-N+1:t}^L \in \mathbb{R}^{L_n \times m}$  from the same data sequence used in  $H_{t-N+1:t}^L$ . By applying the SVHT formula in Eq.(11), on the Page matrix, we can estimate the singular value threshold  $\tau^*$  and approximate the

<sup>5</sup>To avoid confusion with superscript  $L$ , we use  $(A)^L$  to denote the matrix created by raising  $A$  to the power of  $L$ .

<sup>6</sup>If the elements of  $A$  (with  $B = (A)^L$ ) and  $z_0$  in Lemma 1 are drawn from a reasonable distribution, the condition holds with probability one.

effective rank of  $P_{t-N+1:t}^L$  as

$$\hat{r} = \#\{i \in \{1, \dots, Ln_x\} : \varsigma_i \geq \tau^*\} \quad (12)$$

where  $\{\varsigma_i\}_{i=1}^{Ln_x}$  are the singular values of  $P_{t-N+1:t}^L$ .

It is important to note that the rank  $\hat{r}$  estimated via Page SVHT is not fixed but evolves as the sliding window advances. As the buffer shifts, the local data distribution changes, and the singular spectrum captures the instantaneous richness of the underlying dynamics. Consequently, small fluctuations or occasional variations in  $\hat{r}$  are to be expected. Far from being a drawback, this adaptivity ensures that the thresholding remains sensitive to regime shifts and transient behaviors, ultimately producing more reliable models when the system exhibits greater dynamical complexity.

Sec. III-D also yields a conservative local noise-variance estimate. Singular values below the cutoff in Eq. (11) are treated as noise, while those above define the rank via Eq. (12). Let  $\varsigma_{\text{med}}$  be the median singular value of the *Page* matrix with aspect ratio  $\beta$  and  $m$  columns, and let  $\mu_\beta$  denote the median of the Marchenko–Pastur law [37] at aspect ratio  $\beta$ . Then the noise variance  $\hat{\sigma}^2$  can be conservatively estimated as  $\hat{\sigma}^2 \approx \varsigma_{\text{med}}^2 / \mu_\beta m$ . Under the assumption of i.i.d. sensor noise, we approximate the delay-state noise covariance as  $\hat{\nu} \approx \hat{\sigma}^2 I_{Ln_x}$ . This approximation treats each delay state as being perturbed by independent, isotropic noise, which is appropriate in the i.i.d. setting but may underestimate correlations in more structured noise processes. A concrete example of leveraging such variance information within a risk-aware framework is provided in [39].

3) *Cadzow Algorithm*: Now, by using the rank estimate  $\hat{r}$  in Eq.(12) and utilizing Lemma 1, we can finally apply the Cadzow algorithm in Sec.III-C on Hankel matrix  $H_{t-N+1:t}^L$  with effective rank  $\hat{r}$  until we approximate a denoised Hankel matrix which we denote by  $\hat{H}_{t-N+1:t}^L$ .

### B. Online Identification and Multi-Step Prediction

With the denoised Hankel matrix  $\hat{H}_{t-N+1:t}^L$  obtained, we proceed to model the system dynamics using Hankel-DMD. However, as mentioned earlier, to connect the behavior of the dynamics learned by Hankel-DMD in Eqs.(4)-(5) to the system's global behavior via Koopman operator, one often requires assumptions of ergodicity on the system and access to very long trajectories. These assumptions rarely hold in robotics applications. To circumvent this issue, we apply an adaptive sliding window strategy to build a linear model for each buffer and update it as we receive new data.

Formally, let  $\hat{H}_{t-N+1:t-1}^L$  and  $\hat{H}_{t-N+2:t}^L$  be the Hankel matrices constructed by taking the first and last  $N - L$  columns of  $\hat{H}_{t-N+1:t}^L$  respectively.

We then solve a least Frobenius-norm problem similar to Eq. (4) as:

$$\hat{A}_t = \arg \min_{A_t} \|\hat{H}_{t-N+2:t}^L - A_t \hat{H}_{t-N+1:t-1}^L\|_F \quad (13)$$

with the closed-form solution

$$\hat{A}_t = \hat{H}_{t-N+2:t}^L (\hat{H}_{t-N+1:t-1}^L)^\dagger. \quad (14)$$

We then define the local predictor dynamics as

$$\psi_{m+1} = \hat{A}_t \psi_m, \quad m \in \{t, t+1, \dots\}. \quad (15)$$

If we initialize the system (15) by setting  $\psi_t$  to be equal to the last column of  $\hat{H}_{t-N+2:t}^L$  (which corresponds to the denoised version of the lifted state at the current time), we can forecast the future outputs of system (1) by running the predictor (15) and extracting the last block of the delay embedded state as

$$\bar{x}_{t+j} = D (\hat{A}_t)^j \psi_t^* \quad j \in \{1, \dots, N_h\}, \quad (16)$$

where  $\psi_t^*$  is set to be the last column of  $\hat{H}_{t-N+2:t}^L$  and matrix  $D \in \mathbb{R}^{n_x \times Ln_x}$  is defined as  $D = [0_{n_x \times (L-1)n_x}, I_{n_x}]$ .

At the next time step, we advance the buffer to  $\mathcal{B}_{t+1} = \{x_{t-N+2}, \dots, x_{t+1}\}$  and repeat the aforementioned procedure to produce a time-varying sequence of linear predictors characterized by  $\{\hat{A}_t\}_{t \geq N}$ . These predictors are well suited for Model Predictive Control (MPC) by providing linear predictions over the planning horizon. Algorithm 1 compiles the full sliding-window procedure.

---

#### Algorithm 1: Adaptive Sliding-Window Page–Hankel DMD Predictor

---

**Input:** Embedding window  $L$

Buffer Length  $N = mLn_x$  with  $m \geq Ln_x$

Buffer  $\mathcal{B}_t = \{x_{t-N+1}, \dots, x_t\}$  with  $x_t \in \mathbb{R}^{n_x}$

Prediction horizon  $N_h$

**Output:** Denoised Hankel  $\hat{H}_{t-N+1:t}^L$

Model  $\hat{A}_t$  and Forecasts  $\{\bar{x}_{t+1}, \dots, \bar{x}_{t+N_h}\}$

Noise covariance estimate  $\hat{\nu}$

**(1) Page & SVHT:** Form  $P_{t-N+1:t}^L$  per Eq. (3)

Compute SVD  $P_{t-N+1:t}^L = U \text{diag}(\varsigma_i) V^\top$ .

Set  $\beta = (Ln_x)/m$  and  $\varsigma_{\text{med}} = \text{median}\{\varsigma_i\}$

Set cutoff  $\tau^* = \lambda^*(\beta)/\sqrt{\mu_\beta}$  via Eq. (11)

$\hat{r} \leftarrow \#\{i : \varsigma_i \geq \tau^*\}$  per Eq. (12)

**(2) Cadzow Algorithm for  $J$  Iterations:**

$$\hat{H}_{t-N+1:t}^L \leftarrow [\Pi_H \circ \Pi_r]^J (H_{t-N+1:t}^L)$$

**(3) Hankel Partitions and Predictor at  $t$ :**

$$\hat{H}_{t-N+1:t-1}^L, \hat{H}_{t-N+2:t}^L$$

$\hat{A}_t = \hat{H}_{t-N+2:t}^L (\hat{H}_{t-N+1:t-1}^L)^\dagger$  as per Eq. (14)

**(4) Prediction ( $N_h$  steps):** Let  $\psi_t^*$  be the last

column of  $\hat{H}_{t-N+2:t}^L$ . For  $j = 1, 2, \dots, N_h$ ,

$$\bar{x}_{t+j} = D (\hat{A}_t)^j \psi_t^* \text{ per Eq. (16)}$$

**(5) Noise Variance Estimation:** With  $m$  Page

columns and MP median  $\mu_\beta$ , set  $\hat{\sigma}^2 = \varsigma_{\text{med}}^2 / (\mu_\beta m)$  and  $\hat{\nu} = \hat{\sigma}^2 I_{Ln_x}$ .

**(6) Slide Window:**  $\mathcal{B}_{t+1} \leftarrow \{x_{t-N+2}, \dots, x_{t+1}\}$  and repeat (1)–(5).

---

## V. SIMULATIONS AND EXPERIMENTS

We apply Algorithm 1 to validate the proposed framework in both simulations and real-world experiments. Our evaluation focuses on (i) signal-to-noise (SNR) separability, (ii)

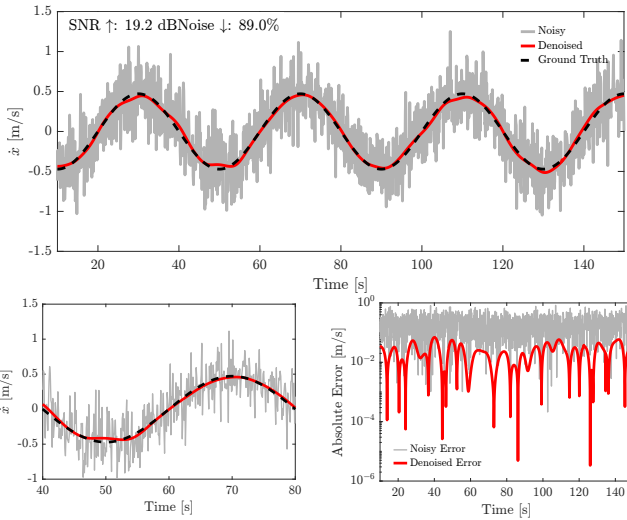


**Fig. 1.** Gaussian noise: Top: noisy (gray), denoised (red) and ground truth (black dashed); call-outs show SNR improvement and average noise reduction. Bottom: zoomed segment and log-scale error.

noise variance estimation, (iii) multi-step prediction accuracy for downstream planning and control applications.

#### A. Simulation: Noisy Unicycle

Consider a reference unicycle model  $\dot{x} = u_1 \cos \theta, \dot{y} = u_1 \sin \theta, \dot{\theta} = u_2$ , [40], [41], which serves as a dynamic obstacle moving along a figure-eight trajectory of amplitude  $a = 3\text{ m}$  and period  $T = 40\text{ s}$ . An ego agent seeks to reach its goal while avoiding collisions with the unicycle, but has access to only noisy velocity measurements of the unicycle rather than the full state. Sampling the reference trajectory at  $\Delta t = 0.02\text{ s}$  yields the forward velocity profile  $u_1^*(t)$ . We inject sensor noise from two distributions: (i) i.i.d. Gaussian,  $\eta_k \sim \mathcal{N}(0, \sigma_x^2)$  with  $\sigma_x = 0.25\text{ m/s}$  and (ii) correlated heavy-tailed AR(1)-Laplace,  $\eta_t = \rho \eta_{t-1} + w_t$ ,  $w_t \sim \text{Laplace}(0, b)$ ,  $|\rho| < 1$ . For fair comparison,  $b$  is chosen so that the stationary variance matches the Gaussian case,  $\text{Var}[\eta_t] = \sigma_x^2$ , i.e.  $b = \sqrt{(1 - \rho^2)\sigma_x^2/2}$ . In both cases, the noisy measurement stream is  $v_t = u_1^*(t) + \eta_t$ .

**Denoising results (Gaussian):** Fig. 1 demonstrates that our Page-Hankel SVHT framework achieves stable recovery of the ground-truth velocity profile under Gaussian sensor noise. The denoised estimate (red, top panel) tracks the ground truth (dashed black) without visible phase lag while suppressing high-frequency artifacts that often contaminate raw measurements. Over the 160 s trajectory, the method delivered an SNR gain of 19.2 dB and an average noise reduction of 89.0% (call-out, top-left), corresponding to nearly an order-of-magnitude improvement over baseline. The zoomed view (bottom-left) highlights that turning points and low-curvature segments, often degraded by conventional low-pass filters, were preserved, while the log-scale absolute error confirms a 10-100 $\times$  reduction in residual magnitude. These results indicate that the method can denoise aggressively without compromising structural features critical for downstream control.

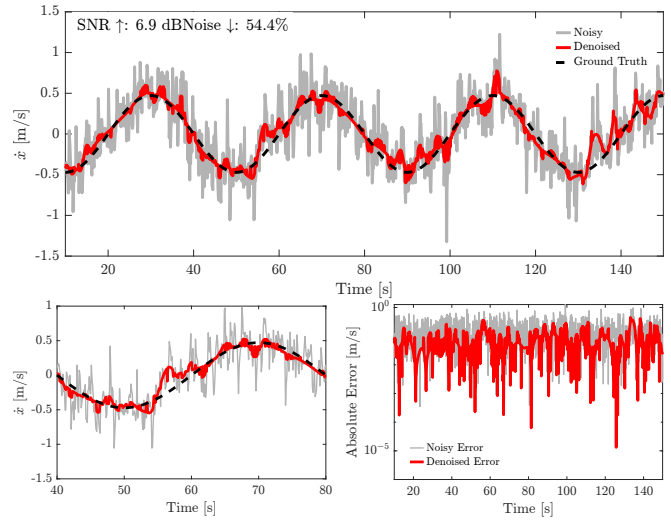


**Fig. 2.** AR(1)-Laplace noise: The denoising algorithm remains effective under heavy-tailed, correlated disturbances: call-outs: SNR +6.9 dB and 54.4% noise reduction.

**Denoising results (Heavy tailed, correlated noise):** To probe robustness under non-Gaussian disturbances, we injected temporally correlated AR(1)-Laplace noise (Fig. 2). Despite heavy tails and temporal correlation, the framework remained comparably effective where we observed an SNR gain of 6.9 dB and an average noise reduction of 54.4%, with no visible phase lag relative to the ground truth. While the performance degraded relative to the Gaussian baseline, as expected under correlated, heavy-tailed disturbances, the degradation was gradual. Crucially, the low-rank Hankel structure proved distribution-agnostic i.e., the SVHT adaptively trimmed outlier-inflated singular values without requiring fixed gaussian assumptions on the noise statistic.

#### B. System Hardware and Experiments

This section validates the full pipeline on hardware. Our experiment in Fig. 3 is motivated by a naval application. Currently, payloads are loaded into their silos by a ship-board crane while the ship docks in a port, where no ocean swells affect the safety of the loading process. It would be desirable to load these payload units into their silos while the ship is underway, potentially in heavy seas. However, in active sea states, the ship sways about with the ocean swells. Anticipating deck motion would enable the controller to compensate during payload delivery.

The testbed is a scaled crane mounted on an *E2M eMove eM6-300-1500* five-DoF Stewart platform that can reproduce wave-induced ship motions. A VN-100 IMU measures linear accelerations and angular velocities of the simulated heaving deck at 30 Hz. Using these measurements, the framework generates 2.0 s i.e., 31-step horizon forecast. This setup enables two evaluations: (i) whether the variance-stable denoising observed in simulation persists under real IMU noise and (ii) whether short-horizon sliding window Hankel-DMD predictions remain within a bounded threshold suitable for MPC integration. Fig. 4 (top) shows a representative trajectory where  $N = 250$  sample context buffer (gray) feeds

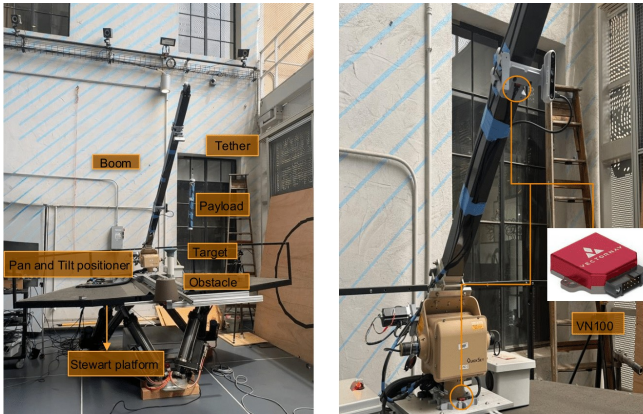


**Fig. 3.** Stewart-platform testbed. **Left:** Moving-base crane with target, obstacle, payload, and arm/tip cameras. **Right:** Base-mounted VectorNav VN-100 IMU supplying orientation and angular rates to the sliding window Hankel-DMD predictor.

the pipeline, generating 31-step forecasts (red) aligned with the ground truth (dashed black). The open-loop predictor achieves an RMSE of 0.012 m/s.

Given a fixed error-tolerance  $\varepsilon = 0.04$ , we define a violation-duration metric on the prediction error  $e_t$  as

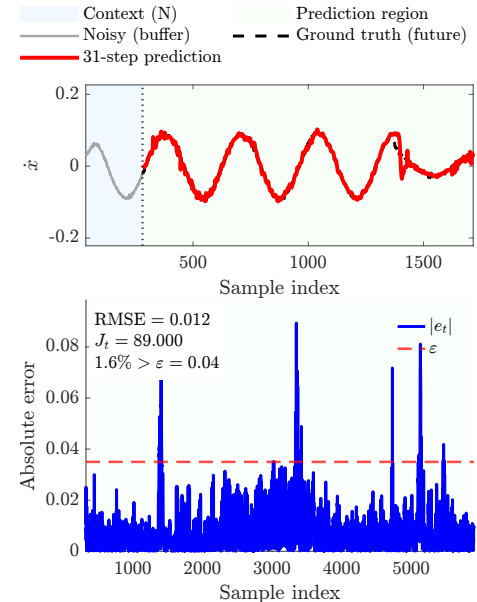
$$J_t = \Delta t \sum_{t=1}^{N_h} \mathbf{1}(e_t \geq \varepsilon), \quad \text{with } e_t := \|\bar{x}_t - x_t\|_2$$

where  $N_h$  defines the prediction horizon,  $\bar{x}_t$  the prediction forecast,  $x_t$  the measured ground truth,  $\Delta t$  the sample period, and  $\mathbf{1}(\cdot)$  the indicator (1 if the condition holds, 0 otherwise). In Fig. 4 (bottom),  $J_t = 89.0$  s (1.6% of horizon<sup>7</sup>), certifying that prediction errors are bounded within the tolerance for 98.4% of the time.

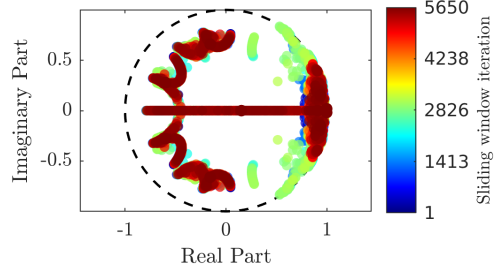
Further investigation of Fig. 4 (top) reveals occasional transient spikes in the predicted trajectory, after which the forecasts quickly return to a nominal accuracy. These anomalies arise when the local embedding window captures a regime shift or abrupt disturbance, briefly mis-aligning the rank estimate. Importantly, such events are short-lived and self-correct as the sliding buffer refreshes, with the subsequent predictions re-stabilizing around the future measurements. This highlights both the adaptivity and the finite-sample sensitivity of the method, i.e., while transient outliers can occur, the framework consistently recovers without persistent drift.

Fig. 5 illustrates the evolution of the eigenvalues of the learned predictors across sliding windows. As the system behavior changes along the trajectory, the models adapt accordingly, and the eigenvalues shift smoothly while consistently remaining within the unit circle, ensuring Schur stability. The gradual evolution of the spectrum highlights the stability and time-varying nature of the local Hankel-DMD models throughout the experiment.

Together, these results demonstrate that our framework not



**Fig. 4.** Top: context buffer ( $N = 250$ , gray) and 31-step forecasts (red) overlaid with ground truth (black dashed). Bottom: absolute prediction error  $|e_t|$  (blue) compared to threshold  $\varepsilon$  (red dashed).



**Fig. 5.** Evolution of eigenvalue across sliding windows: full spectra with iteration-colored progression.

only denoises real sensor streams but also yields stable and bounded predictions that are suitable for downstream planning and control applications. A real-time demonstration of the moving-base prediction and MPC integration is provided in the supplementary video [42].

## VI. CONCLUSION AND FUTURE WORK

We introduced a Page–Hankel SVHT framework for real-time denoising and short-horizon prediction, yielding stable sliding window Hankel-DMD models from noisy data streams. Simulations (Gaussian and heavy-tailed noise) show variance-stable, distribution-agnostic performance and hardware tests with IMU data produce reliable forecasts that may support downstream control. For future work, we plan to integrate rank-1 updates with exponential smoothing for efficient online adaptation and including tensorized delayed embedding matrices for multi-axis consistency. We also plan to validate our method by integrating the predictions within an MPC framework.

## REFERENCES

[1] M. Gulzar, Y. Muhammad, and N. Muhammad, “A survey on motion prediction of pedestrians and vehicles for autonomous driving,” *IEEE Access*, vol. 9, pp. 137957–137969, 2021.

<sup>7</sup>The fraction of the horizon spent above threshold,  $\% \text{violating} = 100 \times \frac{J_t}{T_{\text{hor}}}$ ,  $T_{\text{hor}} := N_h \Delta t$ .

[2] I. Yaqoob, L. U. Khan, S. M. A. Kazmi, M. Imran, N. Guizani, and C. S. Hong, “Autonomous driving cars in smart cities: Recent advances, requirements, and challenges,” *IEEE Network*, vol. 34, no. 1, pp. 174–181, 2019.

[3] R. Spica, D. Falanga, E. Cristofalo, E. Montijano, D. Scaramuzza, and M. Schwager, “A real-time Game Theoretic planner for autonomous two-player drone racing,” in *Robotics: Science and Systems*, 2018.

[4] D. Hanover, A. Loquercio, L. Bauersfeld, A. Romero, R. Penicka, Y. Song, G. Cioffi, E. Kaufmann, and D. Scaramuzza, “Autonomous drone racing: A survey,” 2023.

[5] P. Fiorini and Z. Shiller, “Motion Planning in dynamic environments using Velocity Obstacles,” *Int. J. Rob. Res.*, vol. 17, no. 7, pp. 760–772, 1998.

[6] J. van den Berg, S. J. Guy, M. C. Lin, and D. Manocha, “Reciprocal n-body Collision Avoidance,” in *Robotics Research (ISRR)*, ser. Springer Tracts Adv. Robot. Springer, 2011, vol. 70, pp. 3–19.

[7] J. van den Berg, M. C. Lin, and D. Manocha, “Reciprocal Velocity Obstacles for Real-Time Multi-Agent Navigation,” in *Proc. IEEE Int. Conf. Robot. Autom. (ICRA)*, 2008, pp. 1928–1935.

[8] S. J. Guy, J. Chhugani, C. Kim, N. Satish, M. C. Lin, D. Manocha, and P. Dubey, “Clearpath: Highly parallel collision avoidance for multi-agent simulation,” in *Proc. ACM SIGGRAPH/Eurographics Symp. Comput. Animation (SCA)*, 2009, pp. 177–187.

[9] J. van den Berg, J. Snape, S. J. Guy, and D. Manocha, “Reciprocal Collision Avoidance with Acceleration-Velocity Obstacles,” in *Proc. IEEE Int. Conf. Robot. Autom. (ICRA)*, 2011, pp. 3475–3482.

[10] H. Goldstein, C. Poole, and J. Safko, *Classical Mechanics*, 3rd ed. Addison-Wesley, 2002.

[11] F. Camara, N. Bellotto, S. Cosar, F. Weber, D. Nathanael, M. Althoff, J. Wu, J. Ruenz, A. Dietrich, G. Markkula, A. Schieben, F. Tango, N. Merat, and C. Fox, “Pedestrian models for autonomous driving part ii: High-level models of human behavior,” *IEEE Trans. Intell. Transp. Syst.*, vol. 22, no. 9, pp. 5453–5472, Sep. 2021.

[12] D. Hennes, D. Claes, W. Meeussen, and K. Tuyls, “Multi-robot collision avoidance with Localization Uncertainty,” in *Proc. Int. Conf. Autonomous Agents and Multiagent Systems (AAMAS)*, 2012, pp. 147–154.

[13] N. E. D. Toit and J. W. Burdick, “Robotic Motion Planning in Dynamic, Cluttered, Uncertain environments,” in *Proc. IEEE Int. Conf. Robot. Autom. (ICRA)*, 2010, pp. 966–973.

[14] P. Huang, W. Liu, L. Ma, W. Liang, and Z. Liu, “Auto Regressive Moving Average (arma) modeling method for Gyro random noise using a Robust Kalman Filter,” *Sensors*, 2015.

[15] S. J. Talukder, Y. Yue, and G. Gkioxari, “Totem: Tokenized Time Series Embeddings for General Time Series Analysis,” *Trans. Mach. Learn. Res.*, 2024.

[16] V. Saxena, M. Bronars, N. R. Arachchige, K. Wang, W. C. Shin, S. Nasiriany, A. Mandlekar, and D. Xu, “What matters in learning from Large-Scale datasets for Robot Manipulation?” in *Proc. Int. Conf. Learn. Represent. (ICLR)*, 2025.

[17] H. A. Pierson and M. S. Gashler, “Deep learning in robotics: A review of recent research,” *Adv. Robot.*, Jul 2017.

[18] J. Ko and D. Fox, “GP-Bayesfilters: Bayesian Filtering using Gaussian Process Prediction and Observation Models,” in *Proc. Robotics: Sci. Syst. (RSS)*, 2007.

[19] C. D. McKinnon and A. P. Schoellig, “Context-aware cost shaping to reduce the impact of model error in safe, Receding Horizon Control,” in *Proc. IEEE Int. Conf. Robot. Autom. (ICRA)*, 2020, pp. 2386–2392.

[20] B. O. Koopman, “Hamiltonian Systems and Transformation in Hilbert Space,” *Proc. Natl. Acad. Sci. U.S.A.*, 1931.

[21] P. J. Schmid and J. Sesterhenn, “Dynamic Mode Decomposition of numerical and experimental data,” in *APS Div. Fluid Dyn. (DFD) Meeting*, 2008.

[22] M. O. Williams, I. G. Kevrekidis, and C. W. Rowley, “A Data-Driven approximation of the Koopman Operator: Extending Dynamic Mode Decomposition,” *J. Nonlinear Sci.*, 2015.

[23] H. Arbabi and I. Mezić, “Ergodic Theory, Dynamic Mode Decomposition, and Computation of Spectral Properties of the Koopman Operator,” *J. Nonlinear Sci.*, 2017.

[24] M. Kamb, E. Kaiser, S. L. Brunton, and J. N. Kutz, “Time-Delay Observables for Koopman: Theory and applications,” *SIAM J. Appl. Dyn. Syst.*, 2020.

[25] M. Korda and I. Mezić, “Linear predictors for nonlinear dynamical systems: Koopman Operator meets model predictive control,” *Automatica*, 2018.

[26] C. Folkestad, D. Pastor, and J. W. Burdick, “Episodic Koopman learning of nonlinear robot dynamics with application to fast multirotor landing,” in *Proc. IEEE Int. Conf. Robot. Autom. (ICRA)*, 2020, pp. 9216–9222.

[27] H. Abdi and L. J. Williams, “Principal Component Analysis,” *Wiley Interdiscip. Rev. Comput. Stat.*, 2010.

[28] G. Berkooz, P. Holmes, and J. L. Lumley, “The Proper Orthogonal Decomposition in the analysis of turbulent flows,” *Annu. Rev. Fluid Mech.*, 1993.

[29] M. Yin and R. S. Smith, “On Low-Rank Hankel matrix denoising,” *IFAC PapersOnLine*, 2021.

[30] N. Halko, P.-G. Martinsson, and J. A. Tropp, “Finding structure with randomness: Probabilistic algorithms for constructing approximate matrix decompositions,” *SIAM Rev.*, 2011.

[31] J.-N. Juang and R. S. Pappa, “An Eigensystem Realization Algorithm for Modal Parameter Identification and Model Reduction,” *J. Guid. Control Dyn.*, 1985.

[32] N. Golyandina, V. Nekrutkin, and A. Zhigljavsky, *Analysis of Time Series Structure: SSA and Related Techniques*. Chapman and Hall/CRC, 2001.

[33] F. Takens, “Detecting Strange Attractors in Turbulence,” in *Dyn. Syst. Turbulence*, ser. Lect. Notes Math. Springer, 1981, pp. 366–381.

[34] J. A. Cadzow, “Signal Enhancement – a composite property mapping algorithm,” *IEEE Trans. Acoust., Speech, Signal Process.*, 1988.

[35] C. Eckart and G. Young, “The Approximation of One Matrix by Another of Lower Rank,” *Psychometrika*, 1936.

[36] M. Gavish and D. L. Donoho, “The Optimal Hard Threshold for Singular Values is  $4/\sqrt{3}$ ,” *IEEE Trans. Inf. Theory*, 2014.

[37] V. A. Marčenko and L. A. Pastur, “Distribution of Eigenvalues for Some Sets of Random Matrices,” *Math. USSR-Sb.*, 1967.

[38] L. J. Gleser, “Estimation in a Multivariate Errors in Variables Regression Model: Large Sample Results,” *Ann. Stat.*, 1981.

[39] S. X. Wei, “Data-Driven Safety-Critical Autonomy in Unknown, Unstructured, and Dynamic Environments,” Ph.D. dissertation, California Inst. Technol., 2024.

[40] G. Klancar, A. Zdesar, S. Blazic, and I. Skrjanc, *Wheeled Mobile Robotics: From Fundamentals Towards Autonomous Systems*. Butterworth-Heinemann, 2017.

[41] M. Aicardi, G. Casalino, A. Bicchi, and A. Balestrino, “Closed-loop steering of unicycle-like vehicles via Lyapunov techniques,” *IEEE Robot. Autom. Mag.*, 1995.

[42] S. B. Kombo, “Real-time predictive motion compensation for a moving base using hankel-dmd-based mpc,” YouTube video, 2025, available at <https://youtu.be/-IiIOwDXR1k>.

## APPENDIX

*Proof of Lemma 1.* Given the definition of system and the initial condition, one can write  $x_i = C(A)^i z_0$  for  $i \in \{0, \dots, N-1\}$ . Therefore, one can easily decompose the Page and Hankel matrices as

$$P^L = EF, \quad H^L = EG, \quad (17)$$

where

$$\begin{aligned} E &= [C^\top, A^\top C^\top, \dots, ((A)^{L-1})^\top C^\top]^\top \in \mathbb{R}^{(n_x L) \times n_z}, \\ F &= [z_0, Bz_0, (B)^2 z_0, \dots, (B)^{d-1} z_0] \in \mathbb{R}^{n_z \times d}, \\ G &= [z_0, Az_0, (A)^2 z_0, \dots, (A)^{(d-1)L} z_0] \in \mathbb{R}^{n_z \times ((d-1)L+1)}. \end{aligned}$$

Note that by the hypothesis,  $\text{rank}(F) = n_z$ , which implies that  $F$  has full row rank. Moreover, noting that  $B = (A)^L$ , one can easily see that all columns of  $F$  are in the set of columns of  $G$ ; hence,  $\text{rank}(G) \geq \text{rank}(F) = n_z$ . However, note that  $G \in \mathbb{R}^{n_z \times ((d-1)L+1)}$  has more columns than rows; therefore, its rank can be at most  $n_z$ . Hence, one can conclude that both  $F$  and  $G$  have full row rank and

$$\text{rank}(F) = \text{rank}(G) = n_z. \quad (18)$$

Moreover, using (17), the rank equality (18), and noting that  $\text{rank}(E) \leq n_z$  (due to its size) one can write

$$\begin{aligned}\text{rank}(P^L) &\leq \min(\text{rank}(E), \text{rank}(F)) = \text{rank}(E), \\ \text{rank}(H^L) &\leq \min(\text{rank}(E), \text{rank}(G)) = \text{rank}(E).\end{aligned}\quad (19)$$

On the other hand, Sylvester's rank inequality gives

$$\begin{aligned}\text{rank}(P^L) &= \text{rank}(EF) \geq \text{rank}(E) + \text{rank}(F) - n_z, \\ \text{rank}(H^L) &= \text{rank}(EG) \geq \text{rank}(E) + \text{rank}(G) - n_z.\end{aligned}\quad (20)$$

Inequalities (19)-(20) in conjunction with (18) lead to  $\text{rank}(P^L) = \text{rank}(H^L) = \text{rank}(E)$  concluding the proof.  $\square$